

CHEMISTRY

A European Journal

A Journal of



Accepted Article

Title: Synthesis, Thermal, and Optical Properties of Tris(5-aryl-1,3,4-oxadiazol-2-yl)-1,3,5-triazines, New Star-shaped Fluorescent Discotic Liquid Crystals

Authors: Natalie Tober, Thorsten Rieth, Matthias Lehmann, and Heiner Detert

This manuscript has been accepted after peer review and appears as an Accepted Article online prior to editing, proofing, and formal publication of the final Version of Record (VoR). This work is currently citable by using the Digital Object Identifier (DOI) given below. The VoR will be published online in Early View as soon as possible and may be different to this Accepted Article as a result of editing. Readers should obtain the VoR from the journal website shown below when it is published to ensure accuracy of information. The authors are responsible for the content of this Accepted Article.

To be cited as: *Chem. Eur. J.* 10.1002/chem.201902975

Link to VoR: <http://dx.doi.org/10.1002/chem.201902975>

Supported by
ACES

WILEY-VCH

Synthesis, Thermal, and Optical Properties of Tris(5-aryl-1,3,4-oxadiazol-2-yl)-1,3,5-triazines, New Star-shaped Fluorescent Discotic Liquid Crystals

N. Tober,^[a] T. Rieth,^[a] M. Lehmann^{*[b]} and H. Detert^{*[a]}

Dedicated to Prof. Dr. Herbert Meier, Mainz, on the occasion of his 80th birthday

Abstract: The synthesis of 'TOTs', C₃-symmetrical star-shaped mesogenes with a 1,3,5-triazine centre, 5-phenyl-1,3,4-oxadiazole arms and various peripheral alkoxy side chains is reported. Threefold Huisgen reaction on a central triazine tricarboxylic acid and suitable aryltetrazoles yields the title compounds. Selected analogues with a benzene centre are included in this study and allow an evaluation of the impact of the central unit on physical properties. Thermal (DSC, POM), optical (UV-Vis, fluorescence), electric (TOF) and structural (single crystal, WAXS) properties of these compounds are investigated. The modification of alkoxy chain length and substitution pattern allows a tuning of physical properties. TOTs emit blue to yellow light, depending on conjugation length, donor-acceptor substitution and solvent polarity, whereas concentration quenches, aggregation enhances the emission. The width of the mesophases is typically around $\Delta T = 100 - 150$ K but can even exceed 220 K. Polarization optical microscopy and X-ray diffraction on oriented filaments reveal that TOTs are highly ordered LCs with long range hexagonal columnar structure.

Introduction

The development of new materials for electronic and opto-electronic devices, e.g (NLO)-absorbers, emitters, and semiconductors for the application in solar cells, LEDs, FETs and quantum computers is a highly active research field with an extraordinary commercial potential.^[1-4]

Especially organic compounds are of great interest, they are required to replace rare, toxic and expensive inorganic materials.^[3,5] Organic opto-electronic devices were developed already, like organic photovoltaics (OVPs)^[6], organic light emitting diodes (OLEDs)^[7] and organic field effect transistors (OFETs)^[8]. Whereas calamitic liquid crystals are the key compound in LCDs^[2,8,9], the technology of discotic liquid crystals

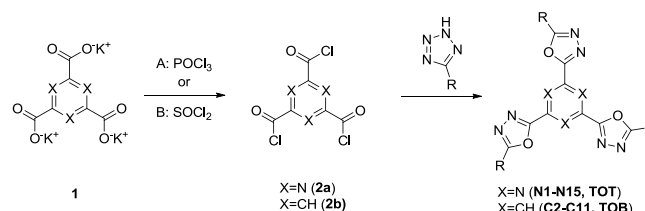
(DLC) is only in its beginning.^[10,11] Further interesting features of DLCs are self-assembly, mostly to formation of columnar mesophases, self-healing, and aggregation-induced emission enhancement.^[12] The columnar arrangement provides the ability of an one dimensional charge transfer^[4,10] by overlapping of the aromatic π -orbitals (" π -stacking").^[13] The majority of DLCs consists of an electron-rich aromatic core, for example triphenylene, (triazatriene, or thiophene, often with electron-rich arms like alkoxybenzene or thiophene.^[9,14,15] In contrast, electron-deficient heterocycles like pyrimidines, triazines or oxadiazoles are less common as components of the π -conjugated core.^[13, 16-18]

1,3,5-Tris-(5-phenyl-1,3,4-oxadiazol-2-yl)benzene (TOB), one of the first reported discotic oxadiazole compounds^[19] melts at 335°C without any liquid crystalline phase, but a few molecules of this structure with flexible side chains attached are reported to form broad mesophases with the characteristic textures of a columnar arrangement, as observed by polarisation optical microscopy (POM).^[20,21]

The exchange of benzene with 1,3,5-triazine leads to a new core for discotic liquid crystals: tris(aryloxadiazolyl)triazine (TOT, **N1 - N15**, scheme 1, fig. 1), a fluorescent scaffold with excellent tendency towards columnar arrangement in the LC phase and broad mesophases. The synthesis, thermal, optical and luminescent properties of these compounds and some benzene analogues (TOBs **C2 - C11**) and the comparison of their properties are subject of this report.

Synthesis and Investigations

Synthesis



Scheme 1. Huisgen reaction: (13 –72%)

The common route to 1,3,4-oxadiazoles is the stepwise formation of diacylhydrazine followed by dehydration/cyclization with POCl₃.^[21-23] This method has been successfully applied for the synthesis of star-shaped molecules with a benzene center. An alternative way to construct oxadiazoles is opened by the Huisgen reaction of tetrazoles and acid chlorides in presence of pyridine bases.^[20,24,25] This method is particularly rewarding for

[a] Natalie Tober, Dr. Thorsten Rieth, Prof. Dr. Heiner Detert, Institute of Organic Chemistry University of Mainz Duesbergweg 10 - 14 55128 Mainz, Germany E-mail: detert@uni-mainz.de

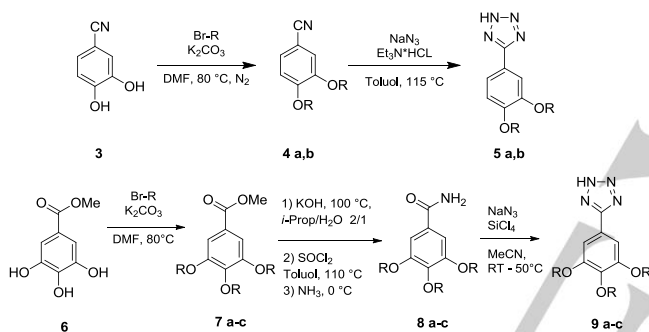
[b] Prof. Dr. Matthias Lehmann, Institute of Organic Chemistry University of Würzburg Am Hubland 97074 Würzburg, Germany

Supporting information for this article is given via a link at the end of the document.

the preparation of sensitive products.^[26] Hence, we followed this strategy to build discotic LCs with a tris-1,3,4-oxadiazolyl-1,3,5-triazine nucleus **N1** - **N15** (scheme 1).

Initial results were disappointing, upon addition of tris(chlorocarbonyl)triazine **2a** to the tetrazole/collidine mixture, a brown precipitate was formed and tetrazoles were converted to nitriles (mass spectrometry). Since the acid chloride **2a** decomposed in the presence of bases and no oxadiazole was formed, the reaction has to be performed in the absence of bases in spite of some side reactions due to HCl. Good yields of heterocyclic stars **N1** - **N15** were obtained, accompanied by small amounts of 1,2,4-triazoles as byproducts (NMR, MS).

The required triazine acid chloride **2a** was prepared in three steps by acid catalysed trimerization of ethyl cyanofornate, saponification, and chlorination of the tripotassium salt **1** with POCl₃ to obtain pure **2a** in 71 % yield after distillation (method A). Similar results in the Huisgen reaction were obtained when **1** was converted to **2a** with thionyl chloride and excess chlorinating agent was evaporated (method B).^[28] It appeared to be essential that **2a** was prepared immediately before the Huisgen reaction.



Scheme 2. Synthesis of tetrazoles.

The tetrazoles (scheme 2) were synthesized in multistep reactions starting with protocatechuic nitrile **3** or methyl gallate **6**.^[29,30] 3,4-(Dialkoxyphenyl)-tetrazoles **5a,b** are accessible via alkylation of **3** and 1,3-dipolar cycloaddition of azide.^[29] The 3,4,5-analogues **9a-c** were synthesized from methyl gallate **6** via alkylation, saponification, chlorination/ammonolysis (SI) followed by dehydration/ azide transfer with triazidochlorosilane.^[31]

Biphenyl tetrazole **10** is accessible via Suzuki cross-coupling reaction of iodophenyl tetrazole and di(decyloxy)phenyl boronic acid.^[32] 5,6-Di(decyloxy)naphth-2-yl-tetrazole **11** was prepared by oxidation of 6-bromo-2-naphthol to the *o*-quinone, reduction, alkylation and Rosenmund-von-Braun cyanation followed by azide addition similar to a literature procedure.

With these tetrazoles in hand, 14 different trisaryloxadiazolyltriazines (TOT, **N1-N15**) and four trisoxadiazolylbenzenes (TOB, **C2 – C4, C9**) were synthesized in yields ranging from 13% up to 72% (figure 1, table 1). Triazoles are formed as by-products, their chromatographic behavior is generally very similar to the tris(oxadiazolyl) stars. Therefore, excessive chromatography is occasionally required - and responsible for reduced yields. Residual triazole in the yellow fluorescent TOT can easily be distinguished by its blue fluorescence on solvent-loaded TLC plates. The identity and

purity of all materials is demonstrated by standard analytical methods, such as ¹H-, ¹³C-NMR, TLC and HR-MS.

For the synthesis of the carbon-analogues **C2 – C9**, trimesic acid trichloride **2b** in the presence of 2,4,6-collidine was a successful protocol, the pure TOBs were obtained in yields up to 61% after chromatography.

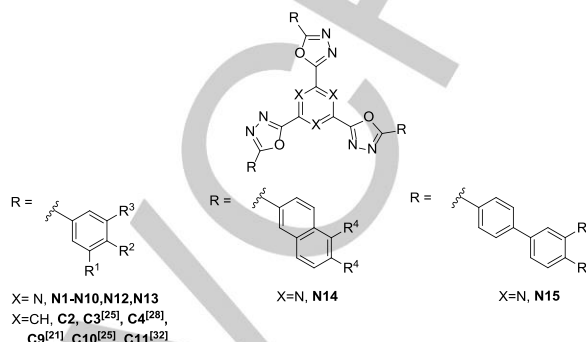


Figure 1. Synthesized compounds and analogues from literature.

Table 1. Tris(aryl-1,3,4-oxadiazolyl)triazines and -benzenes, substitution pattern, chain length, yield and references. (Yields over 2 steps)

	R	Y	R	Y
N1	R ¹ = R ³ = H, R ² = n-propyloxy	47% [A]	N8	R ¹ = R ² = R ³ = n-hexyloxy 31% [B]
N2	R ¹ = H, R ² = R ³ = n-octyloxy	48% [A]	N9	R ¹ = R ² = R ³ = n-octyloxy 34% [A]
C2	R ¹ = H, R ² = R ³ = n-octyloxy	61%	C9	R ¹ = R ² = R ³ = n-octyloxy 13% 28% ^[21]
N3	R ¹ = H, R ² = R ³ = n-decyloxy	38% [A]	N10	R ¹ = R ² = R ³ = n-decyloxy 45% [A]
C3	R ¹ = H, R ² = R ³ = n-decyloxy	59% D ^[23]	C10	R ¹ = R ² = R ³ = n-decyloxy D ^[23]
N4	R ¹ = H, R ² = R ³ = n-dodecyloxy	47% [A]	C11	R ¹ = R ² = R ³ = n-dodecyloxy D ^[27]
C4	R ¹ = H, R ² = R ³ = n-dodecyloxy	33% 87% ^[25]	N12	R ¹ = R ² = R ³ = 2-ethylhexyloxy 55% [B]
N5	R ¹ = H, R ² = R ³ = n-tetradecyloxy	70% [B]	N13	R ¹ = R ² = R ³ = 3,7-dimethyloctyloxy 72% [B]
N6	R ¹ = H, R ² = R ³ = 4-ethyloctyloxy	52% [B]	N14	R ⁴ = n-decyloxy 46% [B]
N7	R ¹ = H, R ² = R ³ = 3,7-dimethyloctyloxy	29% [B]	N15	R ⁵ = n-decyloxy 49% [B]

[A] Method A: C₃N₃(COOK)₃, POCl₃. [B] Method B: C₃N₃(COOK)₃, SOCl₂, [C] trimesic acid chloride; [D] Yield not given in literature. Compounds **C3**, **C4** and **C9** have been reported in the literature and were newly synthesized for this study.

Thermal properties: DSC and POM

Polarized optical microscopy revealed birefringent mesophases for 18 out of 20 star-shaped molecules (including 2 mesogens from literature^[23,27]) under investigation. The LC-phases show textures, typical for hexagonal-columnar arrangements (Fig. 2, a,b). A standard discotic liquid crystal shows usually two transitions in a DSC heating scan - melting and clearing. TOTs and TOBs are highly viscous liquid crystals in the high temperature range as evidenced by shearing experiments. Upon cooling, the structure and texture of the mesophase is maintained, even after complete congealing. Therefore, determination of the melting point is hard to observe by POM. In highly viscous mesophases (TOTs and TOBs), crystallization can be slow, resulting in partial or complete preservation of the mesophase structure. As a consequence, measured melting enthalpies in the cooling scan are lower than those of the first heating cycle. Thus data in table 2 are values for not completely relaxed materials. These phenomena have been observed for several TOTs and TOBs (**N2 - N8, N14, C2, C3**). The partial recrystallization can give rise to a cold crystallization just below the melting point during the subsequent heating scan (**N5, N7, N14**). Glass transitions were detected for **N12** and also transitions between crystal phases (**N15, C3, C9**) which occur only in the first heating curve or after prolonged storage. TOTs **N6** and **N8** are strongly inhibited in crystallization, a second measurement of the same DSC-sample after 2 months did not exhibit any Cr→M transitions, only after two years a DSC experiment revealed a signal attributed to such a transition. Furthermore some TOTs show exothermic transitions in their second heating cycles (e.g. **N5**, figure 3) caused by thermally induced crystallization.^[33] This is followed by two endothermic transitions, melting ($T = 88.5 \text{ }^\circ\text{C}$, $\Delta H = 46.0 \text{ kJ}\cdot\text{mol}^{-1}$) and clearing ($T = 184.3 \text{ }^\circ\text{C}$, $\Delta H = 3.9 \text{ kJ}\cdot\text{mol}^{-1}$).

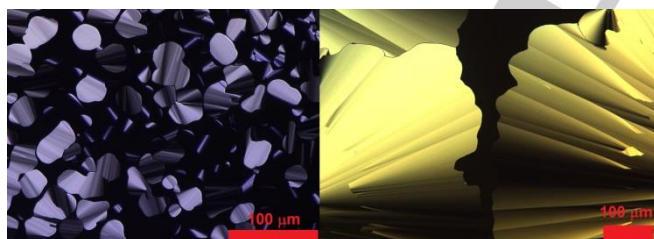


Figure 2. a) POM: fan texture of (**N8**) at 200°C (0.5 K/min) upon cooling b) POM: focal conic fan texture of (**N2**) at 195°C (10 K/min) upon cooling

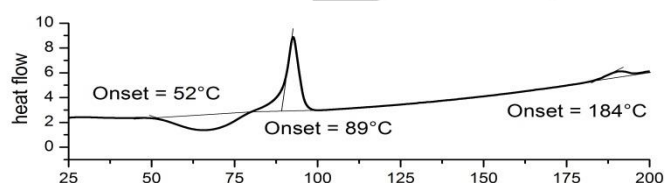


Figure 3. DSC: second heating curve of (**N5**)

The results of POM and DSC investigations on TOTs and TOBs are collected in figure 4 and table 2. TOTs and TOBs show broad mesophases with phase widths of 69-220 K. Generally, the triazine based compounds possess lower melting and higher clearing temperatures than their carbon analogous and

consequently the mesophase ranges are 20 - 64K larger (figure 4). Transition temperatures of 3,4-dialkoxy TOTs **N2-N5** are weakly affected by elongation of alkyl chains (octyl - tetradecyl); maximum T_c is reached with decyl and dodecyl chains. T_c is more influenced by chain length than T_m . The sensitivity of transition points to chain length is more pronounced in the 3,4,5-trialkoxy series **N8-N10**. Compared to the 3,4-dialkoxy derivatives, their LC phases are much broader (up to 220 K!) and appear at significantly lower temperatures.

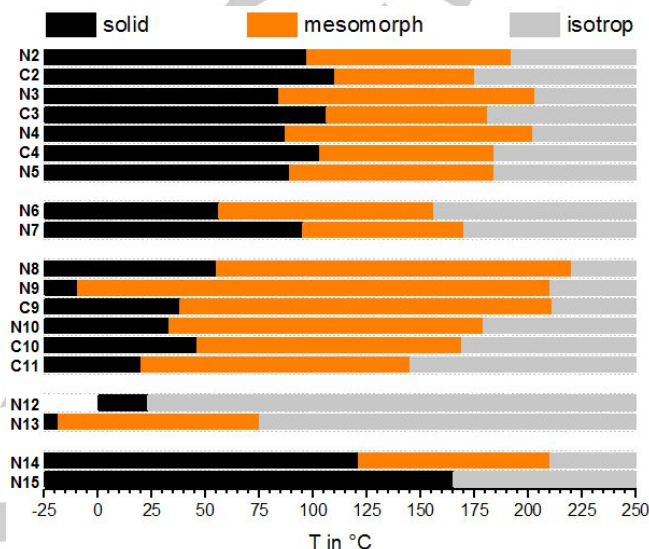


Figure 4. Overview of phase width of tris(aryloxadiazoxy)arene stars

Table 2. Phase transition temperatures ($^\circ\text{C}$) and corresponding enthalpies ($\text{kJ}\cdot\text{mol}^{-1}$)

Compound	Compound	Compound	Compound
N1	Cr 276 I	N8	Cr 55 [24.8] ^c M 220 [1.2] ^c I
N2	Cr 97 [3.7] ^b Col _h 192 [3.4] ^b I	N9	Cr -10 [Tg] ^b Col _h 210 [4.5] ^b I
C2	Cr 106 [67.1] Col _h 181 [4,8] I	C9	Cr 1 [8.0] Cr 34 [20.9] Col _h 190 [4.9] I
N3	Cr 84 [3.9] ^b M 203 [4.3] ^b I	N10	Cr 33 [21.9] ^a M 179 [4.0] ^b I
C3 ^[23]	Cr 51 [92.7] Cr 83 [189.6] Cr 107 [26.7] M 176 [18.4] I	C10 ^[23]	Cr 46 [86.2] M 169 [15.5] I
N4	Cr 87 [3.4] ^b M [4.9] ^b 202 I	C11 ^[27]	Cr ca.20 [e] M ca.145 [e] I
C4 ^[25]	Cr 103 [54.4] M 184 [3.9] I	N12	I
N5	Cr 89 [46.0] ^b M 184 [3.9] ^b I	N13	Cr -19 [Tg] ^c M 72 [0.9] ^b I
N6	Cr 56 [2.9] ^c M 156 [2.3] ^c I	N14	Cr 121 [1.9] ^b M 210 [3.0] ^b I
N7	Cr 95 [0.6] ^a M 170 [2.1] ^b I	N15	Cr 93 [4.1] ^b Cr 165 [26.9] ^b I

a) onset of the signal in first heating cycle b) onset of the signal in second heating cycle c) onset of the signal in heating cycle of the second measurement d) absence of mobility (POM), [e] not given in literature

Branching in the alkyl chains of the triazine stars (**N6, N7, N12, N13**) reduces transition temperatures and width of the LC phase.

This effect is more pronounced in the 3,4,5-trialkoxy series, even a complete loss of mesomorphism has been found (**N12**). This can be due to two reasons: diastereomeric mixtures and steric crowding especially for the 3,4,5-trialkoxy series.

Extending the aromatic system of TOTs, from peripheral phenyl (**N3**) to peripheral naphthalene **N14**, results in an increase of the melting point by 37 K and of the clearing point by 7 K. The even longer biphenyl derivative **N15** reveals only a crystalline phase at much lower temperature, which may be attributed to the non-planar structure of this building block and therefore reduced mobility in a column. The thermal behavior (Cr 25(6) Col_h 114 (4) iso) of a thiophene analogue to **N9** and a higher homologue reveals a strong stabilization of the mesophase by the oxadiazole, probably due to CT interactions between electron deficient oxadiazoles and alkoxyphenyl rings.^[34] Similarly, 1,2,3-triazoles stabilize the mesophase, phase widths are in the range of 160 K.^[17]

X-Ray scattering.

Single crystals of *p*-propyloxy-TOT **N1** were obtained via slow evaporation of a solution in toluene.^[35] **N1** crystallizes in triclinic space group P-1 ($a = 8.62 \text{ \AA}$, $\alpha = 89.91^\circ$, $b = 13.59 \text{ \AA}$, $\beta = 85.75^\circ$, $c = 15.79 \text{ \AA}$, $\gamma = 76.78^\circ$) and contains two molecules per unit cell (fig. 5). Crystallographic data exhibit a non-planar molecular structure. In contrast to the expected C_3 -symmetry (Fig. 5), **N1** adopts a "Y"-shaped form since one phenyloxadiazole arm is flipped around the triazine-oxadiazole bond. These rings show a dihedral angle of 16° whereas all other biaryl units are essentially planar ($\theta \leq 1^\circ$). The dihedral angle between the benzenes and oxadiazoles are about $10\text{-}14^\circ$. Furthermore two propyloxy-unit are disordered.

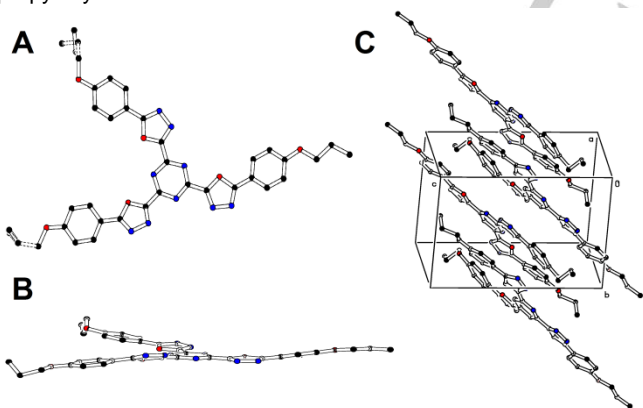


Figure 5. Single crystal structure of **N1** A) asymmetric molecular Y-conformation, B) nearly perfect planarity C) unit cell with alternating arranged molecules.

The broken symmetry has also been observed for a tris-1,2,3-triazolyl-1,3,5-triazine,^[36] but a star similar to **N1** with thiophene replacing oxadiazole^[34,37, 38] shows nearly perfect C_3 -symmetry. This was explained by attractive S-N interactions. The high planarity, dihedral angles between the heterocycles of $1 - 11^\circ$, was found to improve charge transport properties. While these molecules are rotationally displaced with respect to adjacent molecules, the packing of Y-shaped **N1** corresponds to columns

of alternating oriented molecules along a diagonal through the unit cell. Each two molecules have a center of inversion and the central triazines are off-diagonal, bringing oxadiazoles and alkoxyphenyl in close proximity. These features correspond to the results of simulation of the mesophase structure (vide infra).

2D-Scattering on oriented fibres

Two-dimensional wide-angle X-ray scattering (WAXS) experiments on macroscopically aligned extruded fibers were carried out to determine the intra- and intercolumnar organization of the TOTs and TOBs in their liquid crystal phases.

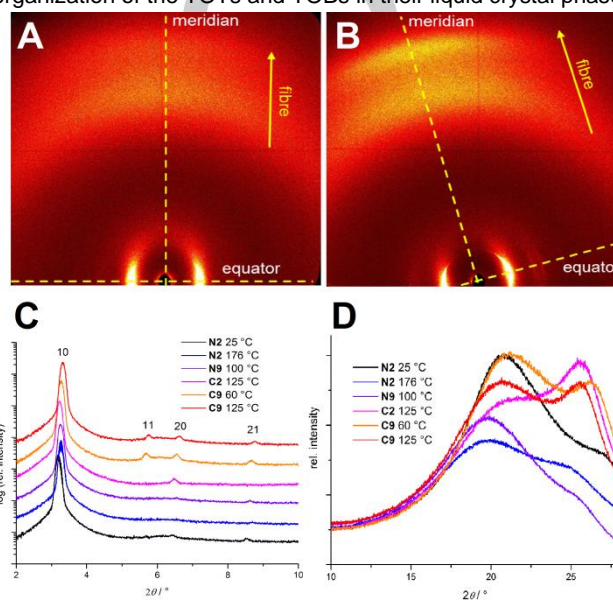


Figure 6: Diffraction pattern of **N2** at 176°C (A) and **C9** at 125°C (B). (C) and (D) show the integrated intensity of the equator and the meridian at various temperatures.

Filaments were obtained by extrusion of **N2**, **N9** in their LC-phase (175°C , 10 min annealing) and of **C2**, **C9** (140°C , 5 min annealing). Table 3 and figure 6 summarise the results. The patterns in Figure 6 (A, B) reveal characteristic features of well-aligned columnar LC samples: (i) reflections centred at the equator attributed to a hexagonal 2D lattice of columns, (ii) a halo corresponding to the liquid-like chains with an average distance between $4.0\text{-}4.6 \text{ \AA}$ (see table 3) and (iii) a rather broad signal at wider angles reminiscent of the average aromatic distances (π - π stacking). The corresponding integration of the patterns along the equator and the meridian (Figure 6 C and D) reveal general trends. First, the reflections with larger and mixed indices are obviously more intense for the carbon derivatives than for the nitrogen derivatives. For **N2** the 11 and 20 reflections appear only at lower temperature. This points to a higher two-dimensional order of columns for the derivatives **C2** and **C9** when compared to **N2** and **N9**. The cell parameters of the hexagonal unit cells decrease with increasing temperature (see also table 3), while simultaneously the distances along the columns increase. However, this effect is surprisingly small since a changes only by 0.7 \AA , when heating **N2** from 25°C to 176°C . These observations are the same for the nitrogen and

the carbon series. The distinct difference in both series is the intensity of the π - π signal corresponding to distances between 3.2-3.5 Å, which is much more intense for the compounds **C2** and **C9** and very small or almost absent for **N2** and **N9**. The correlation length calculated by the Scherrer formula^[39] amounts to 6-7 repeating units for **C2**, **C9** and only about 4 repeating units for **N2** and **N9**. In order to gain more insight in the packing of these star-shaped, shape persistent mesogens the density has been measured at 23.5 °C and extrapolated to the temperatures of the LC phases (table 4, for details see SI).

Table 4. Experimental, extrapolated densities, and number of molecules in a columnar repeating unit h .

#	ρ^A_{exp} / gcm ⁻³	V^B_{mol} / Å ³	V^C_{Ar} / Å ³	V^D_{IAr} (crystal) / Å ³	ρ^E (at T / °C) / gcm ⁻³	Z ^F	columnar repeat h / Å
N2	1.065	2000	698	609	1.02 (100)	3	7.50
N9	1.012	2736	783	625	0.96 (100)	2	6.84
C2	1.029	2065	763	616	0.97 (125)	3	7.68
C9	1.022	2704	751	632	0.95 (125)	2	7.08

A: experimental density at 23.5 °C (buoyancy method) B: molecular volume at 23.5 °C. C: aromatic volume at 23.5 °C D: incremental aromatic volume E: estimated densities at different temperatures (calculation see SI). F: Number of molecules Z in the columnar repeat.

From the density data the molecular volume can be calculated and subsequently the aromatic volumes are available when the known volumes of the aliphatic chains are subtracted.^[40] Here it is evident that all aromatic volumes are larger when compared with the volumes occupied in a crystal, which were calculated by an increment method.^[41] The volumes are 15-25 % higher in the mesophases. This is certainly a consequence of the less dense packing in the soft crystalline and liquid crystalline matter but the large values points also to the fact that the intrinsic free space between the shape-persistent branches cannot be completely filled. There is obviously much less free space in the aromatic part for the derivative **N2** with six chains, which has the highest density. The integer number of molecules filling the columnar repeating h unit (twice the π - π distance) can be calculated to be three molecules for the six chains derivatives and two molecules for the columnar stratum of the nine chain mesogens. For all systems the number of aliphatic chains is identical, the a -parameter is almost identical, too, and therefore the value h must increase for **N2** and **C2** owing to the larger number of aromatic units in the core area of the column. However, this increase amounts only to 0.6-0.7 Å and assuming coplanar stacked mesogens **N2** and **C2** would be only 2.5-2.6 Å apart while for **N9** and **C9** the intramolecular distances are in agreement with π -stacks (3.4-3.5 Å). Since the distances between the six chain derivatives are smaller than van der Waals distances, modelling of the LC phases has been performed in order to unravel packing details. Thus, the columnar phases of **N2**, **N9** and **C9** have been constructed with the program Materials Studio (Forcite, COMPASS II) on the

bases of XRS and density data. Figure 7 highlights the results for compound **N2**. Various starting set-ups with non- C_3 -symmetric and C_3 -symmetric conformers could be geometry optimised to obtain large attractive non-covalent interaction energies after several minimization and annealing procedures. In general, the van der Waals energy was large and negative (-1670 to -1768 kcal/mol, values are given for a set of four unit cells, with 24 molecules), while the electrostatic energy was always positive but decreased slightly when compared with the single molecule (850-898 kcal/mol in the LC phases versus 973 kcal/mol for the single molecule, see SI).

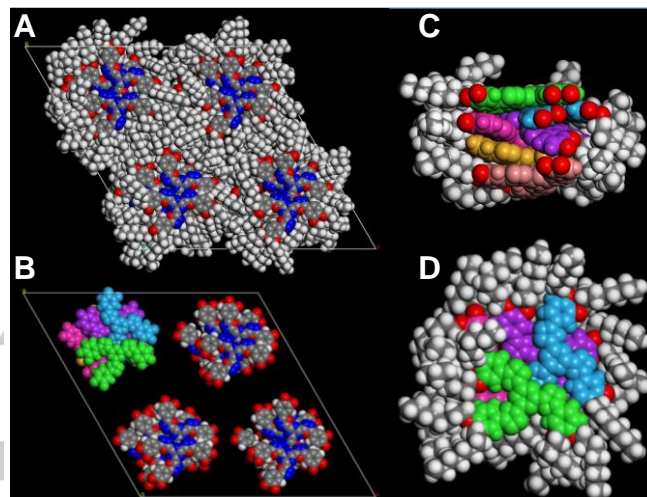


Figure 7: Packing of **N2** in the columnar assembly. Molecules are displaced from the centre of the column and occupy spaces from different columnar slices to fill efficiently the space.

The best results were obtained for the “Y”-shaped conformer similar to the one found in the single crystal. It can be observed, that the core position deviates from the centre of the column (figure 7 C) and that the aromatic units contribute to the space filling of different columnar slices (figure 7 D). The chains densely occupy the peripheral space. As a consequence of this dense packing, the intracolumnar order reduces and almost no π -stacking is visible in the experimental pattern. However, note that **C2**, with the same number of mesogens per columnar stratum must pack in as similar way but nevertheless, exhibit a π stacking signal. Consequently, also the electrostatic repulsion discussed in detail below must be important for the LC self-assembly. When comparing **N9** and **C9** it was apparent that the columnar stratum of height h consists of two molecules with 18 chains and the intracolumnar spacing was calculated to be 3.4 Å (**N9**) and 3.5 Å (**C9**). This can be also confirmed by modelling (see SI). While **C9** shows a clear π -stacking of the mesogens **N9** lacks this signal. The missing π -stacking for **N9** may be explained by the increase in the electrostatic interactions for **N9** compared to single molecules, while for **C9** the electrostatic interactions do not change (see SI).^[42] Thus mesogens **N9** avoid evidently the cofacial stacking.

Electrical conductivity of **N2**, **C2** and **N9**

Conductivity was studied using the Time-of-Flight method to get information of their charge transfer ability (SI). For the 3,4-substituted derivative **N2**, charge carrier mobilities of $\mu = 10^{-3} \text{cm}^2 \text{V}^{-1} \text{s}^{-1}$ in the crystalline (25°C) and mesophase (120°C) are significantly higher as those of its carbon analogue **C2** and the 3,4,5-substituted **N9**, which are in the range of $\mu = 10^{-5} \text{cm}^2 \text{V}^{-1} \text{s}^{-1}$ at 120°C. The latter can be rationalised by the much denser packing of the aromatic scaffold in the centre of the columns when considering **N2** and **N9**. The lower charge carrier mobility of **C2** is not yet well understood, since the aromatic units pack as compact as **N2**, and moreover, show in contrast to **N2** a clear signal for a higher intracolumnar order.

Optical Spectroscopy

Solid tris(oxadiazolyl)triazines are yellow (e.g. branched alkoxy chains) to red (3,4,5-*n*-alkoxy substituted TOTs) compounds whereas the TOBs are colorless. In solution, the latter absorb only in the UV ($\lambda_{\text{max}} \cong 325 \text{ nm}$, $\lambda_{0.1} \cong 360 \text{ nm}$) whereas the absorption bands of TOTs extend into the blue region ($\lambda_{\text{max}} = 360 - 400 \text{ nm}$, $\lambda_{0.1} \cong 406 - 478 \text{ nm}$). A comparison with analogous stars with thiophene^[34,37] or 1,2,3-triazole^[17,18] replacing the oxadiazole in TOTs reveals a similarity between oxadiazole and thiophene stars, the latter absorb at slightly longer wavelengths ($\Delta\lambda \approx 8 \text{ nm}$). On the other hand, UV-spectra of 1,2,3-triazole derivatives peak about $\Delta\lambda \approx -75 \text{ nm}$ at shorter wavelengths.^[34] The excitation maxima of triazine-centered stars (**N1**, **N2**, **N9**, **N14**) in cyclohexane are nearly independent from the analytes' polarity and peak between 380 nm and 385 nm. Only the absorption maximum of biphenyl **N15** is at higher energy ($\lambda_{\text{max}} = 365 \text{ nm}$). Change of solvent has nearly no effect on the absorption spectra, except **N14**, **N15** with the extended π -systems; here, solvatochromic displacements reach $\Delta\tilde{\nu}^{\text{solv}} = 1851 \text{ cm}^{-1}$ (cyclohexane-dichloromethane). Additionally, reduced solubility of some compounds in cyclohexane and acetonitrile provokes turbidity even at 10 μM concentration.

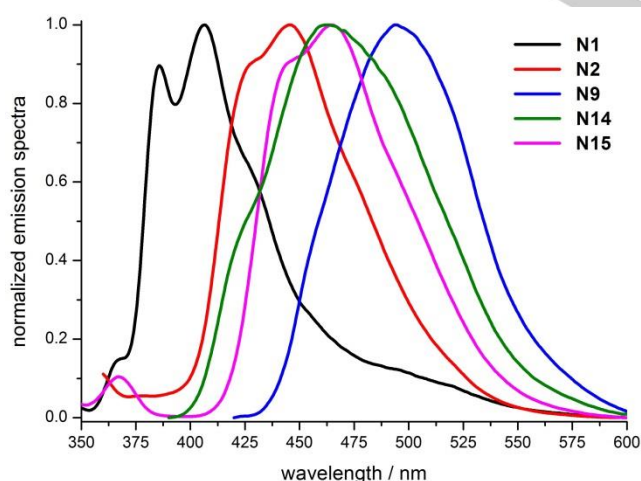


Figure 8. Emission spectra of TOTs with increasing donor substitution (**N1**, **N2**, **N9**) and increasing size of conjugated system (**N2**, **N14**, **N15**) (cyclohexane).

Furthermore, all studied compounds are fluorescent in highly diluted solution in non-polar solvents. The normalized emission spectra of **N1**, **N2**, **N9**, **N15**, and **N14** in cyclohexane are

depicted in figure 6, all other spectra of TOTs and TOBs are given in the supporting information. Like excitation, the emission maxima for TOBs appear at significantly lower wavelengths compared to TOTs (**C3**: $\lambda_{\text{max}} = 326 \text{ nm}$, $\lambda_{\text{max}}^{\text{Fl}} = 396 \text{ nm}$, **N2**: $\lambda_{\text{max}} = 382 \text{ nm}$, $\lambda_{\text{max}}^{\text{Fl}} = 500 \text{ nm}$) and the Stokes shifts are smaller for TOBs ($\Delta\tilde{\nu}_{\text{toluene}}^{\text{St}}(\text{C3}) = 5422 \text{ cm}^{-1} < \Delta\tilde{\nu}_{\text{toluene}}^{\text{St}}(\text{N2}) = 6178 \text{ cm}^{-1}$). The significant shift of excitation and emission maxima to lower energy of 1,3,5-triazine derivatives relative to the benzene analogues is due to the higher acceptor effect of the central electron-deficient triazine. Again, the polarized intramolecular charge distribution causes higher local dipole moments which are more stabilized in polar solvents. Fluorescence quantum yields were determined using quinine sulfate as reference.^[43] The quantum yields of TOTs in highly diluted cyclohexane solution (ca. 0.15 μM) are moderate to high: **N1** (19%), **N2** (64%), **N9** (40%), **N15** (18%), **N14** (27%) and TOBs have even higher quantum yields: **C3** (80%) and **C9** (81%).

Table 4. Optical Spectroscopy

	Solve nt	$\lambda_{\text{max}}/\text{nm}$	$\log\epsilon$	$\lambda_{0.1}/\text{nm}$	$\lambda_{\text{max}}^{\text{F}}/\text{nm}$	$\Delta\tilde{\nu}^{\text{St}}/\text{cm}^{-1}$
N1	CH	380	3.39	nd	407	1746
	Tol	364	4.83	406	450	5250
	DCM	371	4.75	420	478	6034
	AN	356		406	-	
N2	CH	382	4.55	440	446	3756
	Tol	382	4.60	439	500	6178
	DCM	390	4.57	453	-	-
N3	Film	382			581	
N6	Film	382			555	
C3	CH	324	4.81	360	375	4389
	Tol	326	4.84	364	396	5422
	DCM	325	4.83	364	428	7500
	AN	337	4.58	nd	464	7792
	Film	326			409	
N9	CH	380	4.60	438	494	6073
	Tol	379	4.60	437	524	7301
	DCM	383	4.56	451	501	6150
	Film	380			565	
C9	CH	321	4.78	361	390	5772
	Tol	323	4.80	360	419	7093
	DCM	320	4.81	359	462	9466
	Film	-			450	
N14	CH	385	4.45	nd	463	4376
	Tol	394	4.50	452	503	5500
	DCM	401	4.48	478	-	-
	AN	371	4.36	nd	559	8065
N15	CH	362	4.54	nd	465	6119
	Tol	383	4.72	441	519	6842
	DCM	388	4.65	464	-	-
	AN	377	4.72	nd	559	8795

Solvents: CH: cyclohexane; Tol: toluene, DCM: dichloromethane, AN: acetonitrile, $\lambda_{0.1}^F$ = absorption edge at 10% of λ_{max}^F ; nd: not determined due to turbidity

An increasing number of alkoxy substituent (**N1** < **N2** < **N9**) enhances the donor-acceptor character that results in bathochromic shifts of emission maxima. According to the extended π -system of **N15** (biphenyl), and **N14** (naphthyl), their emission peaks appear at slightly lower energies than recorded for the shorter dialkoxyphenyl star **N2**.

Comparison of the emission of TOTs with similar 1,2,3-triazole derivatives reveals that the latter emit at much higher energies (λ_{max}^F = 415 - 471 nm, THF), whereas the thiophene congener of **N9** fluoresces with λ_{max}^F = 528 nm (CH₂Cl₂).^[17,18,34]

With an increasing solvent polarity, the emission maxima are shifted to lower energies, solvatochromic shifts (cyclohexane-dichloromethane) up to $\Delta\tilde{\nu}^{solv}$ = 3650 cm⁻¹ (**N1**) have been recorded. The moderate positive solvatochromism of the emission is accompanied by an efficient fluorescence quenching in polar solvents, e.g. in acetonitrile and even dichloromethane. This effect correlates with increasing donor-acceptor character.

In addition to polarity, concentration has a detrimental effect on the emissivity. THF solutions with triazine star concentrations of ca. 5×10^{-4} M are essentially not emissive. Dilution to 5×10^{-5} M in THF allows a weak emission which increases dramatically upon further dilution to 5×10^{-7} M. Compared to the 'concentrated' (10^{-4} M) solutions, the fluorescence efficiencies increase by a factor of 1.4×10^4 (**N2**) and 2.9×10^4 (**N9**) upon dilution to 10^{-7} M. Though benzene-centered stars are less sensitive to self-quenching, dilution from 5×10^{-4} M to 5×10^{-5} M enhances the fluorescence efficiency by a factor of 45 (**C3**) or 28 (**C9**) but the emission maximum of TOBs is independent from the concentration. However, a diluted solution of **N2** emits with λ_{max}^F = 562 nm, 37 nm more on the red side than a concentrated solution whereas λ_{max}^F of **N9** shifts to the blue, from λ_{max}^F = 440 nm to 422 nm. For investigation of optical properties in the solid state, **N3**, **C3**, **N6**, **N9**, and **C9** with a 3,4- and 3,4,5-substitution pattern and central triazine or benzene ring were studied as representative examples. While films of TOBs and TOTs show absorption maxima very similar to the dyes in solution, the long-wavelength tail of triazine stars brings a yellow (**N6**) or orange-red color (**N3**, **N9**). The impact of the environment on the emission is more pronounced. TOBs emit blue light while the emission of TOTs is yellow (**N9**: λ_{max}^F = 567 nm, $\lambda_{0.1}^F$ = 642 nm; **N3**: λ_{max}^F = 580 nm, $\lambda_{0.1}^F$ = 651 nm).

A comparison of solution and film spectra reveals that the interaction of the π -systems of TOTs strongly affects the emission. While the emission maxima of solid TOBs are blue-shifted compared to dichloromethane solution (**C3**: $\Delta\tilde{\nu}$ = -1025 cm⁻¹, **C9**: $\Delta\tilde{\nu}$ = -676 cm⁻¹), the π - π interaction in solid TOTs gives rise to large bathochromic shifts. These exceed the effect of the polar dichloromethane by $\Delta\tilde{\nu}$ = 2260 cm⁻¹ (**N9**, λ_{max}^F = 565 nm) or even $\Delta\tilde{\nu}$ = 3027 cm⁻¹ (**N2/N3**, λ_{max}^F = 580 nm). Branching in the side chains (**N6**, 4-ethyloctyloxy) requires more space and deranges the π - π interaction, the yellow film emits with λ_{max}^F = 554 nm ($\lambda_{0.1}^F$ = 633 nm). The strong intermolecular electronic interaction of excited **N9** in the solid state is in sharp contrast to the behaviour of the thiophene analogue,^[34] which emits at

higher energies ($\Delta\tilde{\nu}$ = -254 cm⁻¹) compared to dichloromethane solution. Furthermore, the emission of films of TOTs and TOBs is temperature-dependent. (SI) Pristine TOT films emit with λ_{max}^F = 581 nm (**N3**); 555 nm (**N6**), 570 nm (**N9**). Heating into the mesophase (150 °C) provokes significant blue-shifts (λ_{max}^F = 536 nm (**N3**); 538 nm (**N6**), 531 nm (**N9**)). Upon cooling to 25 °C, these maxima lose intensity (**N3**: 15%, **N6**: 15%, **N9**: 23%), whereas the intensity in the long-wavelength shoulder (**N3**: λ = 569 nm, **N6**: λ = 565 nm, **N9**: λ = 570 nm) is not affected. The impact of temperature on the emission of TOTs with linear side chains **N3** ($\Delta\tilde{\nu}$ = 1941 cm⁻¹), **N9** ($\Delta\tilde{\nu}$ = 1288 cm⁻¹) is higher than of **N6** ($\Delta\tilde{\nu}$ = 569 cm⁻¹) with branched chains. A slow reorganization process (**N6** > **N9** > **N3**) shifts the fluorescence back to longer wavelengths.

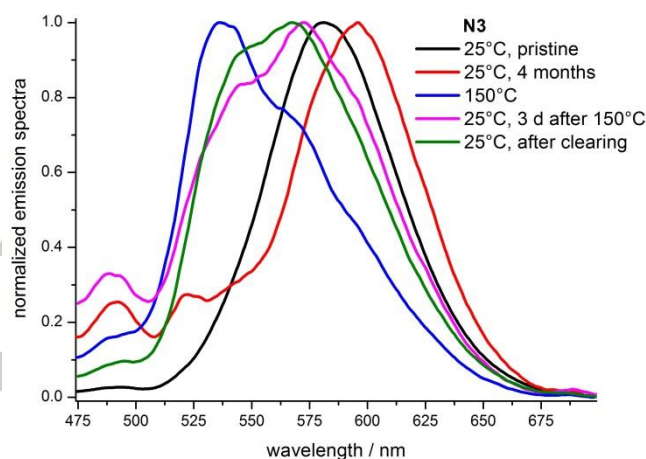


Figure 9. Emission spectra of **N3** with at 150 °C and at 25 °C with different thermal history.

Contrary to the TOTs, only variation of the fluorescence intensity, but no significant spectral changes occurred upon changing the temperature of films of TOBs. A film of **C3** on glass loses about 24% of its emissivity upon cooling from 150 °C to 25 °C. Surprisingly, the same experiment with **C9** gives an initial fluorescence enhancement (24%) upon cooling from 150 °C, followed by reduction of the fluorescence to 87% (at 25 °C) of the initial intensity (150 °C). Here again, in addition to the particular electronic structure, the specific molecular order in the columns controls the electronic properties.

Adding water or heptane as poor solvents to solutions of TOTs (**N2**, **N9**) and TOBs (**C3**, **C9**) in THF results in the formation of aggregates (concentration of stars in all solutions: 0.3 – 0.5 mM). Besides turbidity, the effect on absorption is very individual.

Heptane (up to 90% in THF) has no significant effect on the absorption spectra of **C3**, **C9**, **N9**, but generates a long-wavelength shoulder of **N2** at 470 nm. Water, a highly polar non-solvent (50 - 90%), shifts λ_{max} to the red (≤ 50 nm). The more impressive part is the change of emission behaviour: Whereas the solutions in THF (0.3 - 0.5 mM) are essentially not emissive, the suspensions of aggregates in the mixed solvents are! **N2** (λ_{max}^F = 507 nm) and **N9** (λ_{max}^F = 517 nm) in THF-heptane mixtures emit at lower energies than in THF-water mixtures (**N2**: λ_{max}^F = 470 nm; **N9**: λ_{max}^F = 468 nm), but the opposite is true

for the benzene analogues (**C2**: $\lambda_{max}^F = 390$ (heptane), $\lambda_{max}^F = 413$ nm (water); **C9**: $\lambda_{max}^F = 412$ (heptane), $\lambda_{max}^F = 475$ nm (water)). A comparison of the emission from aggregates and from films reveals that the aggregates of TOTs emit at significantly higher energies than TOTs in solution cast films ($\lambda_{max}^F = 564 - 580$ nm) whereas λ_{max}^F of TOBs in THF/water peak at lower energies.

Obviously, the electronic spectra of these stars, especially those with a triazine center, are strongly controlled by intermolecular interactions. Surprisingly, a concentration quenching of the fluorescence in solution is opposed by aggregation-induced emission. This and the different optical properties of aggregates and films imply a plethora of molecular arrangements of triazine-centered stars.

Conclusions

Two series of discotic molecules composed of three alkoxyaryl-1,3,4-oxadiazolyl arms attached to a benzene center or electron deficient triazine core were synthesized via threefold Huisgen reaction of tetrazoles with trimesic acid trichloride and 2,4,6-tris(chlorocarbonyl)-1,3,5-triazine as central rings. The latter is much more sensitive and requires a modified procedure. Almost all di- and tri-alkoxy substituted TOTs and TOBs exhibited thermotropic mesophases with the characteristic textures of hexagonal columnar arrangements. A variation of chain number and length allows control of the width of mesophase. In general triazine derivatives have broader mesophases ($\Delta T \leq 220^\circ\text{C}$) than benzene analogues ($\Delta T \leq 170^\circ\text{C}$). The mesophases are enantiotropic though several TOTs are crystallization inhibited. X-Ray diffraction and density measurements on oriented fibres proved the dense packing of all derivatives in high temperature hexagonal columnar phases. The 3,4,5-substituted derivatives (**C9**, **N9**) stack with average $\pi - \pi$ distances of 3.4–3.5 Å and with 18 alkyl chains in a columnar stratum of approximately 7 Å height, i.e. with two molecules. While the carbon analogue **C9** show a strong π stacking signal, this is reduced for the triazine derivative **N9**, presumably, because of electrostatic repulsion. In contrast the two chain derivatives **C2** and **N2** contain three molecules in a columnar repeat between 7.5–7.7 Å. Again, the number of chains sum up to 18, but three aromatic cores fill now the centre of the columns, where a coplanar stacking is not anymore possible. For all derivatives a denser packing can be achieved with a Y-shaped conformer of the star, minimising the intrinsic free space.^[44]

The charge carrier mobilities of TOBs and TOTs ($\mu = 10^{-3} - 10^{-5} \text{cm}^2\text{V}^{-1}\text{s}^{-1}$) are in the medium range of discotic liquid crystals.

TOBs are colourless and TOTs are yellow to red coloured substances, their emission behaviour is largely controlled by intermolecular interactions. Efficient emission in highly diluted solution, concentration quenching, aggregation induced emission (enhancement) and sensitivity of the emission spectrum to solvents, temperature, and aggregation are optical phenomena that complement the thermal mesomorphism.

Experimental Section

Synthetic procedures, analyses, spectra, and equipment are collected in the Supporting Information

Acknowledgements

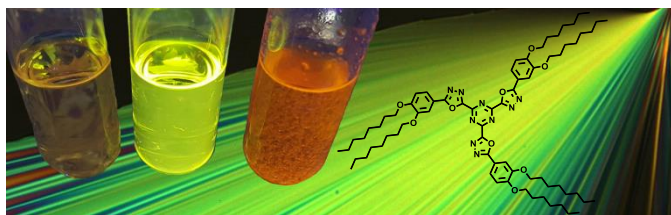
The authors gratefully acknowledge Dr. Johannes Liermann (NMR), Prof. Dr. F. Laquai (ToF), M. Müller (DSC) and Dr. C. Kampf (MS), Dr. D. Schollmeyer (Single Crystal X-Ray Scattering), the Deutsche Forschungsgemeinschaft (DE 515/9-1) for partial funding and the Carl-Zeiss Stiftung for a generous fellowship (N. Tober).

Keywords: discotic liquid crystal • fluorescence • heterocycle • mesophase • star-shaped compound • conjugated Oligomers • solvatochromism • X-ray scattering • aggregation induced emission

- [1] B. Roy, N. De, K. C. Majumdar, *Chem. Europ. J.* **2012**, *18*(46), 14560–14588.
- [2] S. Laschat, A. Baro, N. Steinke, F. Giesselmann, C. Hägele, G. Scalia, R. Judele, E. Kapatsina, S. Sauer, A. Schreivogel, M. Tosoni, *Angew. Chem. Int. Ed.* **2007**, *46*(26), 4832–4887.
- [3] V. Balzani, G. Bergamini, P. Ceroni, *Angew. Chem. Int. Ed.* **2015**, *54*(39), 11320–11337.
- [4] S. Kumar, *Chemistry of discotic liquid crystals: From monomers to polymers*; CRC Press, Boca Raton, FL, **2011**.
- [5] V. Balzani, G. Bergamini, P. Ceroni, *Angew. Chem.* **2015**, *127*(39), 11474–11492.
- [6] a) L. Schmidt-Mende, *Science* **2001**, *293*, 1119–1122; b) C. W. Tang, *Appl. Phys. Lett.* **1986**, *48*, 183; c) I. Seguy, P. Jolinat, P. Destruel, J. Farenc, R. Mamy, H. Bock, J. Ip, T. P. Nguyen, *J. Appl. Phys.* **2001**, *89*, 5442;
- [7] a) W. Pisula, A. Menon, M. Stepputat, I. Lieberwirth, U. Kolb, A. Tracz, H. Sirringhaus, T. Pakula, K. Müllen, *Adv. Mater.* **2005**, *17*, 684–689; b) T. Hassheider, S. A. Benning, M. W. Lauthof, R. Oesterhaus, S. Alibert-Fouet, H. Bock, J. W. Goodby, M. D. Watson, K. Müllen, H.-S. Kitzerow in *Liquid Crystal Materials, Devices, and Applications IX*; (Ed. L.-C. Chien), *Proc. SPIE* **2003**, *5003*, 167–174.
- [8] D. Adam, P. Schuhmacher, J. Simmerer, L. Häußling, W. Paulus, K. Siemensmeyer, K.-H. Etzbach, H. Ringsdorf, D. Haarer, *Adv. Mater.* **1995**, *7*, 276–280.
- [9] B. R. Kaafarani, *Chem. Mater.* **2011**, *23*, 378–396.
- [10] M. Bäker, *Funktionswerkstoffe*; Springer Fachmedien Wiesbaden, Wiesbaden, **2014**.
- [11] a) D. Demus, J. W. Goodby, G. W. Gray, H. W. Spiess, V. Vill, *Handbook of Liquid Crystals*; Wiley, Weinheim, **2011**; b) T. Wöhrle, I. Wurzbach, J. Kirres, A. Kostidou, N. Kapernaum, J. Litterscheidt, J. C. Haenle, P. Staffeld, A. Baro, F. Giesselmann, S. Laschat, *Chem. Rev.* **2016**, *116*, 1139–1241.
- [12] a) S.-H. Wu, H.-H. Chen, *Tetrahedron* **2019**, *75*, 220–229; b) N. Röder, T. Marszalek, D. Limbach, W. Pisula, H. Detert, *ChemPhysChem* **2019**, *20*, 463–469; c) C. Cuerva, J. A. Campo, P. Ovejero, M. R. Torres, E. Oliveira, S. M. Santos, C. Lodeiro, M. Cano, *J. Mater. Chem. C* **2014**, *2*, 9167–9181.
- [13] a) S. Kumar, *Chemical Soc. Rev.* **2006**, *35*, 83–109; b) H. Detert, M. Lehmann, H. Meier, *Materials* **2010**, *3*, 3218–3330.
- [14] a) M. Talarico, R. Termine, E. M. García-Frutos, A. Omenat, J. L. Serrano, B. Gómez-Lor, A. Golemme, *Chem. Mater.* **2008**, *20*, 6589–6591; b) M. Vadivel, I. S. Kumar, K. Swamynathan, V. A. Raghunathan, S. Kumar, *ChemistrySelect* **2018**, *3*, 8763–8769; g) A. Gowda, L. Jacob, D. P. Singh, R. Douali, S. Kumar, *ChemistrySelect* **2018**, *3*, 6551–6560.
- [15] a) J. Luo, B. Zhao, J. Shao, K. A. Lim, H. S. On Chan, C. Chi, *J. Mater. Chem.* **2009**, *19*, 8327; b) H. Taing, J. G. Rothera, J. F.

- Binder, C. L. B. Macdonald, S. H. Eichhorn, *Liq. Cryst.* **2018**, *45*, 1147–1154; c) K.-C. Zhao, J.-Q. Du, H.-F. Wang, K.-Q. Zhao, P. Hu, B.-Q. Wang, H. Monobe, B. Heinrich, B. Donnio, *Chem. Asian J.* **2019**, *14*, 462–470; d) D. Tian, Y. Zhou, Z. Li, S. Liu, J. Shao, X. Yang, J. Shao, W. Huang, B. Zhao, *ChemistrySelect* **2017**, *2*, 8137–8145; e) L. Zhang, D. L. Hughes, A. N. Cammidge, *J. Org. Chem.* **2012**, *77*, 4288–4297.
- [16] a) J. Han, *J. Mater. Chem. C* **2013**, *1*, 7779; b) E. Beltrán, J. L. Serrano, T. Sierra, R. Giménez, *Org. Lett.* **2010**, *12*, 1404–1407.
- [17] a) E. Beltrán, J. L. Serrano, T. Sierra, R. Giménez, *J. Mater. Chem.* **2012**, *22*, 7797–7805; b) B. Feringán, P. Romero, J. L. Serrano, R. Giménez, T. Sierra, *Chem. Europ. J.* **2015**, *21*, 8859–8866.
- [18] a) H. Meier, M. Lehmann, H. C. Holst, D. Schwoeppe, *Tetrahedron* **2004**, *60*, 6881–6888; b) A. Navarro, M. P. Fernández-Liencres, G. García, J. M. Granadino-Roldán, M. Fernández-Gómez, *Phys. Chem. Chem. Phys.* **2015**, *17*, 605–618.
- [19] K. Naito, A. Miura, *J. Phys. Chem.* **1993**, *97*, 6240–6248.
- [20] S. Varghese, N. S. S. Kumar, A. Krishna, D. S. S. Rao, S. K. Prasad, S. Das, *Adv. Funct. Mater.* **2009**, *19*, 2064–2073.
- [21] Y.-D. Zhang, K. G. Jespersen, M. Kempe, J. A. Kornfield, S. Barlow, B. Kippelen, S. R. Marder, *Langmuir* **2003**, *19*, 6534–6536.
- [22] a) T. Curtius, F. H. Dellschaft, *J. Prakt. Chem.* **1901**, *64*, 419–438; b) R. Stollé, H. P. Stevens, *J. Prakt. Chem.* **1904**, *69*, 366–381; c) B. Pradhan, S. K. Pathak, R. K. Gupta, M. Gupta, S. K. Pal, A. S. Achalkumar, *J. Mater. Chem. C* **2016**, *4*, 6117–6130; d) K. Kotwica, A. S. Kostyuchenko, P. Data, T. Marszalek, L. Skorka, T. Jaroch, S. Kacka, M. Zagorska, R. Nowakowski, A. P. Monkman, A. S. Fisyuk, W. Pisula, A. Pron, *Chem. Europ. J.* **2016**, *22*, 11795–11806.
- [23] S. K. Pathak, R. K. Gupta, S. Nath, D. S. S. Rao, S. K. Prasad, A. S. Achalkumar, *J. Mater. Chem. C* **2015**, *3*, 2940–2952.
- [24] a) R. Huisgen, J. Sauer, H. J. Sturm, J. H. Markgraf, *Chem. Ber.* **1960**, *93*, 2106–2124; b) D. D. Prabhu, N. S. S. Kumar, A. P. Sivadas, S. Varghese, S. Das, *J. Phys. Chem. B* **2012**, *116*, 13071–13080.
- [25] E. Giroto, J. Eccher, A. A. Vieira, I. H. Bechtold, H. Gallardo, *Tetrahedron* **2014**, *70*, 3355–3360.
- [26] a) H. Detert, E. Sugiono, G. Kruse, *J. Phys. Org. Chem.* **2002**, *15*, 638–641; b) H. Detert, *Synthesis* **1999**, 999–1004.
- [27] S. H. Gihm, B. G. Kim, S. Kim, J. Seo, S. Y. Park, C. R. Park, *J. Mol. Struct.* **2010**, *984*, 371–375.
- [28] G. Xu, L. Zheng, S. Wang, Q. Dang, X. Bai, *Synth. Commun.* **2010**, *40*, 361–369.
- [29] R. Cristiano, Santos, D. M. Pereira de Oliveira, H. Gallardo, *Liq. Cryst.* **2005**, *32*, 7–14.
- [30] T. Rieth, S. Glang, D. Borchmann, H. Detert, *Mol. Cryst. Liq. Cryst.* **2015**, *610*, 89–99.
- [31] A.-A. S. El-Ahl, S. S. Elmorsy, A. H. Elbeheery, F. A. Amer, *Tetrahedron Lett.* **1997**, *38*, 1257–1260.
- [32] T. Rieth, T. Marszalek, W. Pisula, H. Detert, *Chem. Europ. J.* **2014**, *20*, 5000–5006.
- [33] R. Cristiano, H. Gallardo, A. J. Bortoluzzi, I. H. Bechtold, C. E. M. Campos, R. L. Longo, *Chem. Commun.* **2008**, 5134–5136.
- [34] T. Yasuda, T. Shimizu, F. Liu, G. Ungar, T. Kato, *J. Am. Chem. Soc.* **2011**, *133*, 13437–13444.
- [35] *CCDC 1894806 (N1)* contains the supplementary crystallographic data for this paper. These data can be obtained free of charge from The Cambridge Crystallographic Data Centre via www.ccdc.cam.ac.uk/datarequest/cif.
- [36] A. R. Katritzky, S. K. Singh, N. K. Meher, J. Doskocz, K. Suzuki, R. Jiang, G. L. Sommen, D. A. Ciaramitaro, P. J. Steel, *Arkivoc* **2005**, *2006*, 43–62.
- [37] K. Navamani, K. Senthikumar, *J. Phys. Chem. C* **2014**, *118*, 27754–27762.
- [38] H. Muraoka, M. Mori, S. Ogawa, *Phosphorus, Sulfur, and Silicon and the Related Elements* **2015**, *190*, 1382–1391.
- [39] P. Scherrer, *Nachrichten von der Gesellschaft der Wissenschaften zu Göttingen* **1918**, 98–100.
- [40] B. Donnio, B. Heinrich, H. Allouchi, J. Kain, S. Diele, D. Guillon, D. W. Bruce, *J. Am. Chem. Soc.* **2004**, *126*, 15258–15268.
- [41] A. Immirzi, B. Perini, *Acta Cryst A* **1977**, *33*, 216–218.
- [42] V. Lemaury, D. A. da Silva Filho, V. Coropceanu, M. Lehmann, Y. Geerts, J. Piris, M. G. Debije, A. M. van de Craats, K. Senthikumar, L. D. A. Siebbeles, J. M. Warman, J.-L. Brédas, J. Cornil, *J. Am. Chem. Soc.* **2004**, *126*, 3271–3279.
- [43] J. R. Lakowicz, *Principles of fluorescence spectroscopy*; Springer, New York, NY, **2010**.
- [44] M. Lehmann, M. Dechant, M. Lambov, T. Ghosh, *Acc. Chem. Res.* **2019**, *52*, 1653–1664.

COMMUNICATION



A series of C_3 -symmetrical stars is prepared via Huisgen reaction of alkoxyaryl-tetrazoles and a central tricarboxylic acid. These π -conjugated discotic molecules are solvatochromic fluorophores, a rim of six to nine alkoxy chains provokes broad mesophases.

Natalie Tober, Thorsten Rieth,

Matthias Lehmann^{*} and Heiner Detert^{*}

Page No. – Page No.

Synthesis, Thermal, and Optical Properties of Tris(5-aryl-1,3,4-oxadiazolyl)-1,3,5-triazines, New Star-shaped Fluorescent Discotic Liquid Crystals

Accepted Manuscript